TOPICAL REVIEW — Fundamental physics research in lithium batteries

Mechanics of high-capacity electrodes in lithium-ion batteries*

Ting Zhu†

Woodruff School of Mechanical Engineering, Georgia Institute of Technology, Atlanta, Georgia 30332, *USA*

(Received 15 August 2015; revised manuscript received 14 November 2015; published online 8 December 2015)

Rechargeable batteries, such as lithium-ion batteries, play an important role in the emerging sustainable energy landscape. Mechanical degradation and resulting capacity fade in high-capacity electrode materials critically hinder their use in high-performance lithium-ion batteries. This paper presents an overview of recent advances in understanding the electrochemically-induced mechanical behavior of the electrode materials in lithium-ion batteries. Particular emphasis is placed on stress generation and facture in high-capacity anode materials such as silicon. Finally, we identify several important unresolved issues for future research.

Keywords: lithium-ion batteries, mechanics, electrochemistry, silicon

PACS: 46.50.+a, 62.20.−x, 82.45.Fk **DOI:** 10.1088/1674-1056/25/1/014601

1. Introduction

Energy storage with high performance and low cost is critical for applications in consumer electronics, zero-emission electric vehicles, and stationary power management.[1,2] Lithium-ion batteries (LIBs) are the widely used energy storage systems due to their superior performance.[3] The operation of an LIB involves repeated insertion and extraction of Li ions in active battery electrodes, which are often accompanied with considerable volume changes and stress generation.[4–13] In the development of next-generation LIBs, mechanical degradation in high-capacity electrode materials arises as a bottleneck issue. The high-capacity electrode materials usually experience large volume changes (e.g., up to about 280% for Si), leading to high stresses and fracture in electrodes during electrochemical cycling.[14–23] Fracture causes the loss of active materials and yields more surface areas for solid electrolyte interphase (SEI) growth, both of which contribute to the fast capacity fade of LIBs. In addition, the mechanics issues are prominent at the battery pack and cell levels due to the requirements of structural integrity and crash safety for operating LIBs in hybrid and all electric vehicles.[24]

In this paper, we present an overview of recent advances in studying the mechanics of solid-state electrode materials in LIBs, with an emphasis on fundamentals of stress generation, stress-electrochemistry coupling, and fracture in high-capacity electrode materials such as Si. There are several recent review papers on the phenomenology and mechanisms of lithiation and delithiation in high-capacity electrodes.[20,25,26] Here we present selected examples to highlight the new understanding of coupled electro-chemo-mechanical phenomena as well as the new knowledge of mechanical properties of high-capacity electrodes.

2. Multiscale mechanics of LIBs

The mechanics of LIBs deals with inherently multiscale phenomena. Figure 1 presents a schematic overview of the electro-chemo-mechanical processes occurring at multiple time and length scales in LIBs; also shown are the examples of experimental and modeling studies at different scales. Specifically, at the macroscopic scale, the mechanics problems of the battery pack and cells arise primarily from the requirements of structural integrity and protection under high mechanical loading and severe crashing conditions.[24] For the fundamental research at this scale, thin films are commonly used for studying the mechanical responses and properties of electrode materials under cyclic electrochemical loadings.[9] At the mesoscopic scale, the prominent mechanics problems involve the mechanical behavior of electrodes, which are composed of active storage particles, binders, and electrolytes that fill the pores between storage particles. An effective approach of characterizing the porous microstructures is the x-ray nano-computed tomography.[27] The tomography data enable an evaluation of the porosity and tortuosity of the electrode. They also provide a structural basis of the numerical modeling of the electrochemical and mechanical responses of porous electrodes. At the nanoscale scale, the mechanics of individual electrode particles and wires can be studied in great detail under electrochemical cycling. Particularly, *in situ* transmission electron microscopy (TEM) provides a powerful approach of visualizing the deformation, microstructure evolution, and fracture

*Project support by the NSF (Grant Nos. CMMI 1100205 and DMR 1410936).

†Corresponding author. E-mail: ting.zhu@me.gatech.edu

during lithiation and delithiation of individual or a group of nano-sized electrode materials.[28] At the scales of atoms and electrons, the physical origins of electro-chemo-mechanical coupling need to be studied for understanding the phenomena such as the Jahn–Teller effect on lattice distortion during Li insertion/extraction,[3] the Li-induced embrittlement of carbon materials,[29] etc. To this end, a variety of experimental and modeling tools are commonly used, such as x-ray diffraction, high-resolution TEM, nuclear magnetic resonance (NMR), first-principles calculations, etc.

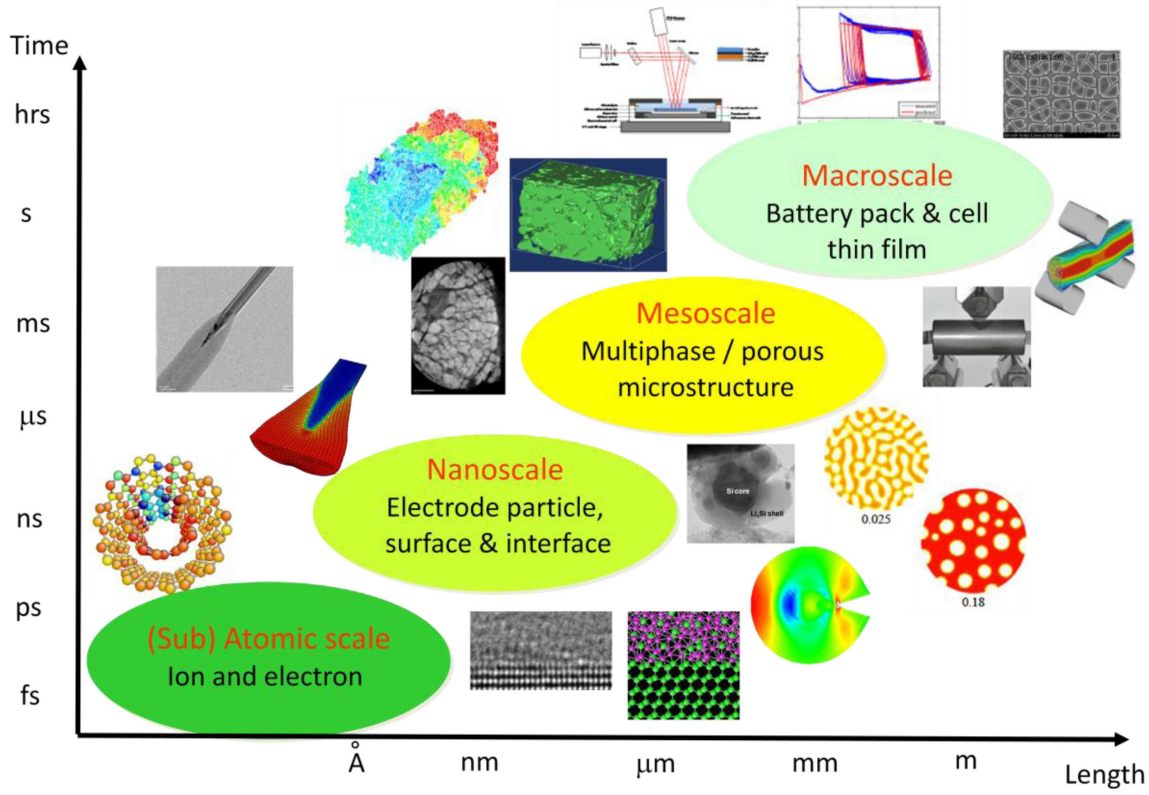

Fig. 1. An overview of the multiscale electro-chemo-mechanics in LIBs.[9,24,27,28]

3. Coupled electro-chemo-mechanical phenomena

The coupled electro-chemo-mechanical phenomena are extremely rich in LIBs. Below we begin with a review of the experimental and modeling studies of stress generation in thin films and particles. Then we proceed to review the recent progress in studying the effects of stress on lithiation kinetics and mechanical degradation in electrodes. These mechanistic studies advance our understanding of the electro-chemo-mechanical processes in LIBs, and they also highlight the critical need for a quantitative characterization of the mechanical properties of electrode materials, which is an important topic that will be reviewed in Section 4.

3.1. Stress generation in lithiated thin films

High-capacity electrode materials typically experience large volume changes during Li insertion and extraction. For the conversion-type anode material such as Si, its lithiation at room temperature usually yields amorphous $Li_{3.75}Si$ (*a*-$Li_{3.75}Si$), resulting in a volume increase of about 280%. Such a large volume expansion can be largely removed upon delithiation. Under constraints, the large volume changes lead to stress generation in the electrode materials. The resulting stresses can be very high, causing plastic flow. Sethuraman *et al.*[9] have used *in situ* wafer-curvature techniques to measure the stress evolution in thin films of *a*-Si during Li insertion and extraction. Figure 2(a) shows the schematic of their experimental setup, where the lithiation and delithiation of an amorphous Si thin film are constrained by a Si wafer substrate with a Cu underlayer in between (acting as a current collector). Figure 2(b) shows the measured galvanostatic discharge and charge curves, and figure 2(c) shows the resultant biaxial stresses in the film. It is seen that during the initial stages of lithiation, the film undergoes elastic loading. At a capacity of about 300 mAh/g, the film yields at a compressive stress of about 1.5 GPa, such that the plastic deformation begins to occur with continuing plastic flow throughout the rest of lithiation. Upon delithiation, a similar elastic–plastic response occurs, resulting in tensile biaxial stresses in the film. These measurements reveal the existence of the high yield stresses and extensive plastic flow during lithiation/delithiation of *a*-Si under constraints.

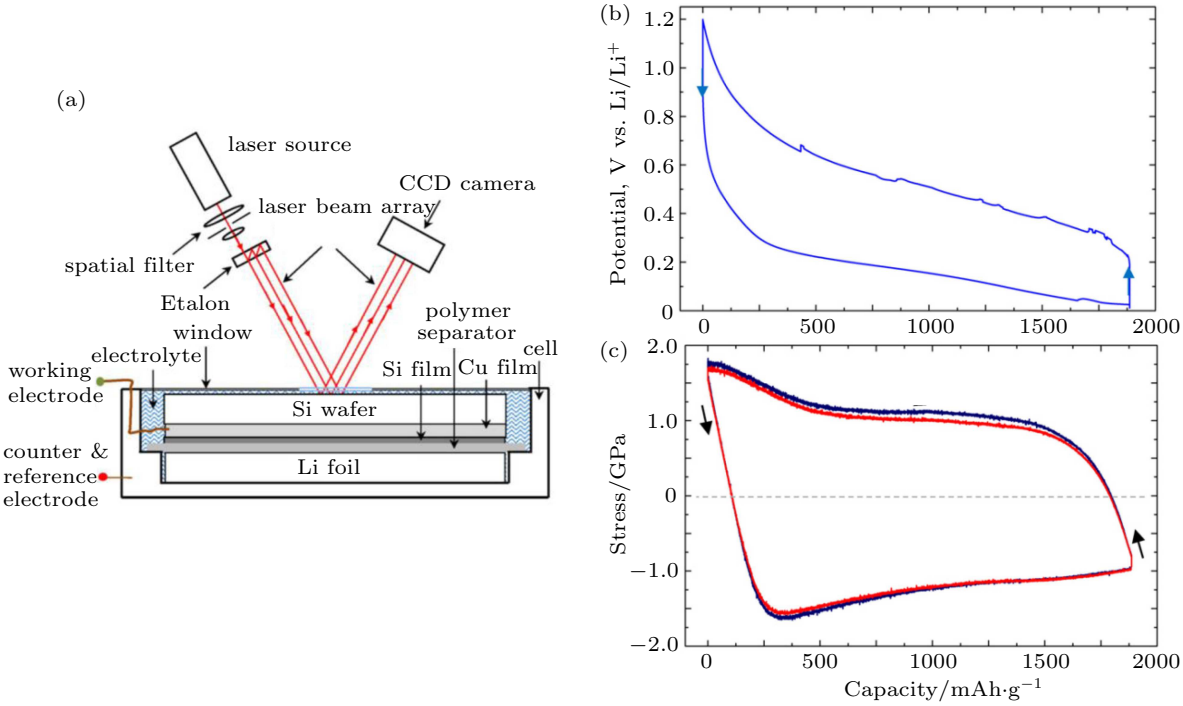

Fig. 2. *In situ* measurement of stress evolution in an *a*-Si thin film during lithiation.[9] (a) Schematic of the *in situ* curvature technique for measuring stresses in lithiated thin film. (b) Cell potential versus capacity curve corresponding to lithiation and delithiation of *a*-Si thin-film electrode cycled at a rate of C/4. (c) Corresponding biaxial stress measured in the film.

3.2. Lithiation-induced stress in particles

Stress generation in particles and wires with curved geometries, which are the common building blocks of electrodes, is different from that in flat thin films. This is because the curvature effect can be significant during stress generation in spherical particles and cylindrical wires, particularly when a two-phase mechanism is involved. *In situ* TEM experiments have shown that the lithiation of Si particles, with either a starting crystalline[17] or amorphous[19] phase, usually proceeds through the formation of a core-shell structure, involving the movement of a two-phase boundary that separates the inner core of pure Si with the outer shell of *a*-Li$_x$Si ($x \sim 3.75$). Such a sharp phase boundary suggests that the Li-poor and Li-rich phases do not transform continuously into each other with changing composition. That is, there is a large solubility gap (i.e., Δx) between the two phases, manifested as an abrupt change of Li concentrations across the phase boundary.

Huang *et al*. have developed a chemo-mechanical model to analyze the stress evolution during two-phase lithiation of a spherical Si particle (Fig. 3(a)).[30] This model accounts for plastic deformation resulting from large lithiation strains. Particularly, it highlights the curvature effect of the sharp phase boundary on stress evolution during lithiation. Figure 3(b) shows two representative results of radial Li distribution, both of which involve a sharp phase boundary with an abrupt change of Li concentration. Figures 3(c) and 3(d) show the simulated radial stress distributions corresponding to the Li profiles in Fig. 3(b). The most significant result from this study is the tensile hoop stress in the surface layer developed as the two-phase boundary moves into the interior of the particle, as seen from Fig. 3(d). Such hoop tension results from a reversal of the initial hoop compression as shown in Fig. 3(c).

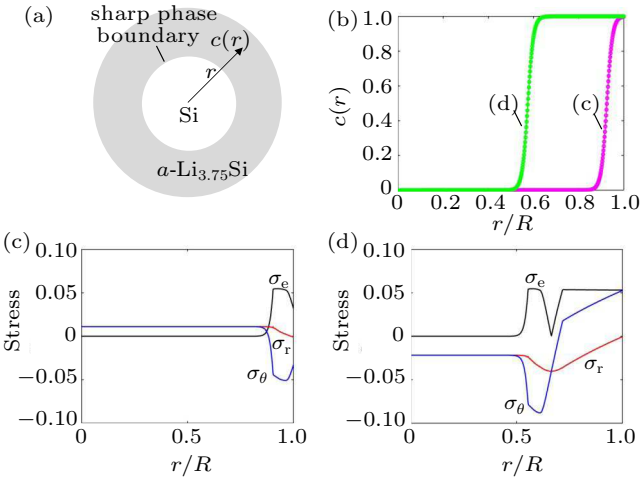

Fig. 3. Modeling of stress generation in a spherical Si particle undergoing two-phase lithiation.[30] (a) Schematic of the two-phase model with a sharp phase boundary between the Si core and *a*-Li$_{3.75}$Si shell. (b) Numerical results showing the radial distribution of Li concentration c normalized by its maximum value at the fully lithiated state, and the radial distance r is normalized by the current radius R of a partially lithiated particle which increases as lithiation proceeds. (c), (d) Numerical results showing the radial distribution of the von Mises effective stress σ_e, radial stress σ_r, and hoop stress $\sigma_\theta = \sigma_\varphi$ (normalized by Young's modulus).

To provide a physical interpretation of the reversal of hoop compression to tension in the surface layer, figure 4 shows the schematics of hoop stresses experienced by a repre-

sentative material element A near the surface. Here the shell is assumed to be fully lithiated with a constant Li concentration. It follows that the lithiation strain should be mainly generated near the moving core–shell interface, where the Li concentration changes abruptly. Figure 4(a) shows that in the early stage of lithiation, element A is located within the pristine core. As lithiation occurs at the reaction front, the newly lithiated material at the front tends to move in the outward radial direction. This arises because there are larger areas in the hoop direction at larger radial distances, where the lithiation-induced volume expansion can be better accommodated with lower stresses generated. The outward displacement of newly lithiated materials results in hydrostatic tension in element A, as represented by stage (a) of the σ_θ curve in Fig. 4(d). As the reaction front sweeps through element A, a large dilational lithiation strain is created at A. Owing to the constraint of surrounding material, local compressive stresses develop, such that element A sequentially undergoes tensile elastic unloading, compressive elastic loading, and compressive plastic yielding in the hoop direction. This stress sequence is schematically represented by stage (b) in Fig. 4(d). Interestingly, as the reaction front continues to move toward the center, the lithiation-induced swelling at the front pushes out the material behind it. This action causes further displacement of element A in the outward radial direction and simultaneously stretches it in the hoop directions. As a result, element A experiences compressive elastic unloading, tensile elastic loading, and tensile plastic yielding, which correspond to stage (c) in Fig. 4(d).

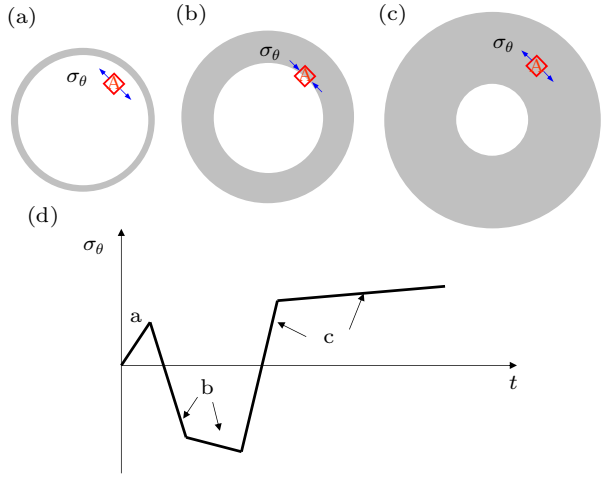

Fig. 4. Illustration of the change of hoop stress σ_θ with time t in a spherical particle, which contains a moving two-phase boundary between the pristine core (white) and lithiated shell (grey).[30] (a)–(c) σ_θ in a representative material element A near the surface. As the phase boundary moves toward the center of the particle, progressive lithiation results in a gradual expansion of the particle, leading to the reversal of hoop compression in panel (b) to hoop tension in panel (c). (d) Schematic plot of σ_θ versus t in element A.

It is important to emphasize that the reversal of hoop compression to tension arises due to the curvature effect of the phase boundary; namely, behind the curved phase boundary, there are larger areas in the hoop direction at larger radial distances. Such reversal will not occur if the phase boundary is flat as in the case of two-phase lithiation in a thin film. More importantly, the high tensile stress and associated tensile plastic flow in the surface layer can cause fracture of electrode particles during Li insertion, which will be discussed in detail in Section 3.4. Finally, we note that for cylindrical wires, a similar conclusion can be drawn for the curvature effect on the reversal of hoop compression to tension in the surface layer of the wires.

3.3. Coupling between stress and electrochemistry

The coupling between electrochemistry and mechanics is usually strong in high-capacity electrode materials. For example, high stresses can be induced during electrochemical lithiation of Si, as discussed in Sections 3.1 and 3.2. Such high stresses, in turn, can affect the rate of lithiation. Liu *et al*. conducted the *in situ* TEM study of lithiation kinetics in a *c*-Si nanowire.[31] Figures 5(a)–5(e) show the evolution of the two-phase, core–shell structure in a *c*-Si nanowire during lithiation. In Fig. 5(f), the measured thickness of the *a*-Li_xSi shell is plotted as a function of time; also plotted are the diameter changes of the Si core and the etched depth, taken from a typical cross section of the Si nanowire. During the lithiation process over 4 hours, the diameter of the *c*-Si core decreases from 139 nm to 101 nm, and the thickness of the *a*-Li_xSi grows from 0 to 54 nm. In the first hour, the lithiation was fast and the average velocity of the core–shell interface was about 10 nm per hour or equivalently 3×10^{-12} m/s. The lithiation apparently slowed down as the core–shell interface moved to the center of the Si nanowire, and became extremely slow after about 2.5 hours. These results clearly demonstrate the self-limiting lithiation in Si nanowires. McDowell *et al*. also reported the slowing of lithiation in *c*-Si nanoparticles as the two-phase reaction front moved to the center of nanoparticles.[32] Recently, Gu *et al.* showed that bending of a Ge nanowire broke the lithiation symmetry, such that lithiation was sped up at the tensile side while slowed down at the compressive side of the nanowire.[33]

The self-limiting lithiation can be reasonably attributed to the retardation effect of lithiation-induced stresses. As discussed in Section 3.2, large compressive stresses can build up in the lithiated shell, owing to the geometrical constraints from the unlithiated *c*-Si core. At this moment, there is a lack of experimentally measured chemo-mechanical properties of Li_xSi such as chemical strains of Li insertion and elasto-plastic properties of Li_xSi, all of which can depend sensitively on Li concentration. As a result, the quantitative stress distribution in lithiated Si cannot be determined. Therefore, it remains an open question whether the self-limiting lithiation is dominantly controlled by the stress-retarded reaction at the

two-phase boundary or the stress-retarded diffusion within the lithiated shell behind the two-phase boundary.

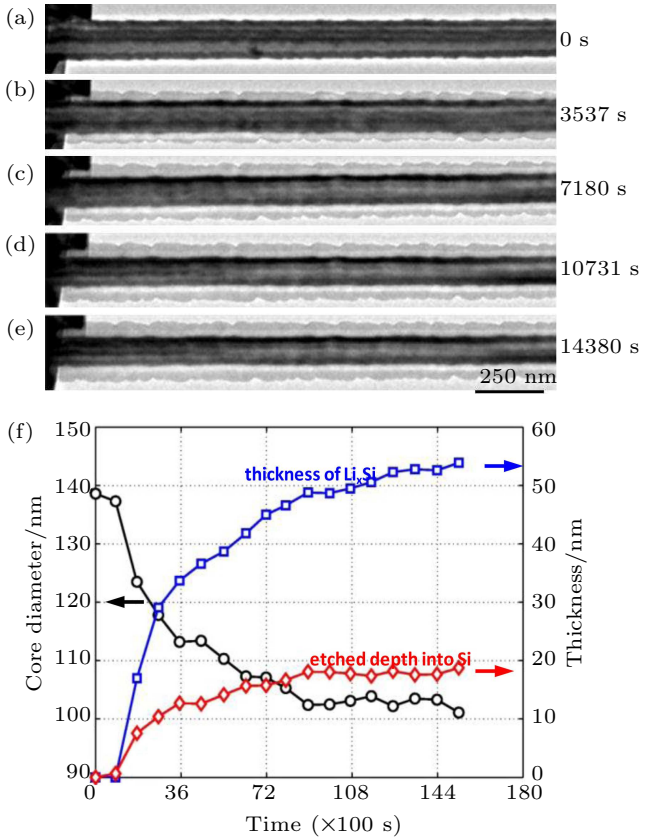

Fig. 5. *In situ* TEM experiment of self-limiting lithiation in a Si nanowire.[31] (a)–(e) Time-lapsed images showing the evolution of the *c*-Si core and *a*-$Li_{3.75}Si$ shell in the nanowire in 4 hours. (f) Plots of nanowire diameter, etched depth, and thickness of the *a*-$Li_{3.75}Si$ shell versus time.

3.4. Size-dependent fracture during lithiation

The electrochemically-induced stresses often cause the mechanical degradation in electrode materials. *In situ* TEM experiments by Liu *et al.*[17] have revealed a strong size dependence of fracture in Si nanoparticles, i.e., there exists a critical particle diameter D_c of $\sim$ 150 nm, below which the particles neither cracked nor fractured upon first lithiation, and above which the particles initially formed surface cracks and then fractured due to lithiation-induced swelling.

Figure 6 shows the *in situ* TEM observation of lithiation responses in a *c*-Si nanoparticle with the initial diameter of about 54 nm, larger than the critical size D_c. This *c*-Si nanoparticle was in contact with a W electrode and a Li metal counter electrode, whose surface was covered with Li_2O acting as a solid electrolyte. Under an applied voltage between the two electrodes, Li quickly covered the particle surface and then diffused radially into the particle, forming the structure of a pristine inner Si core and an *a*-$Li_{3.75}Si$ alloy shell with a sharp interface in between. As the diameter of the Si core shrunk to about 300 nm, the lithiation-induced swelling caused crack initiation from the particle surface. Further lithiation resulted in fragmentation of this nanoparticle. In contrast, figure 7 shows the lithiation of two Si nanoparticles (marked as A and B) with initial diameters of $\sim$ 80 and 40 nm, respectively, which are significantly below the critical size D_c. Both particles underwent the core–shell lithiation process and remained unbroken after full lithiation.

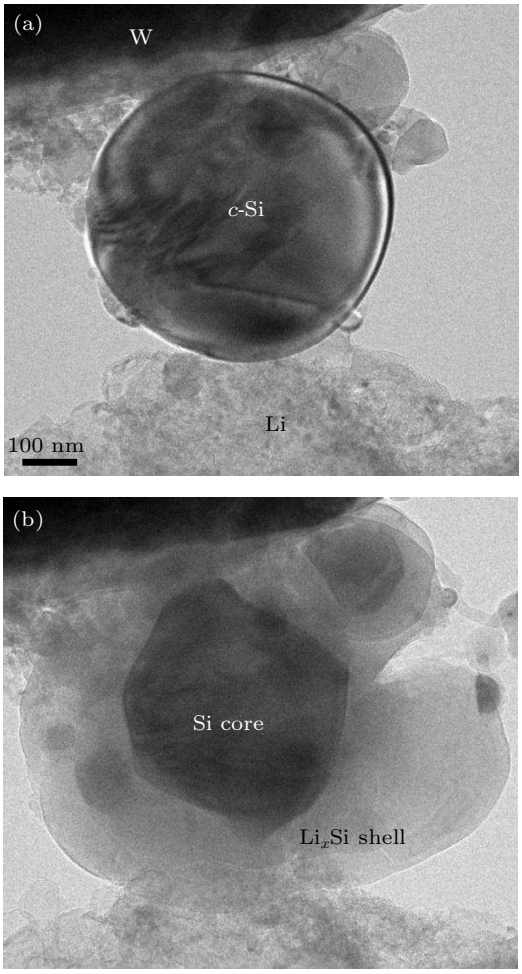

Fig. 6. *In situ* TEM observation of cracking in a *c*-Si nanoparticle during lithiation.[17] (a) A *c*-Si nanoparticle with the initial diameter of 540 nm. (b) A core–shell structure forms as lithiation progresses, and the lithiation-induced swelling causes crack initiation at the particle surface.

Surface cracking in large Si nanoparticles arises due to the buildup of a large hoop tension that reverses the initial compression in the surface layer, as discussed in Section 3.2. While the resulting hoop tension tended to initiate surface cracks, the small-sized nanoparticles nevertheless averted fracture. This is because the stored strain energy from electrochemical reactions is insufficient to drive crack propagation, as dictated by the interplay between the two length scales, i.e., particle diameter and crack size, that control the fracture. More specifically, the crack extension is controlled not only by the high stresses but also by the size of the high-stress region that is dictated by the interplay between two length scales, i.e., particle diameter and flaw size. When a crack-like flaw of length *a* is formed in a large particle, near

the crack faces the lithiation-induced tensile stress is relaxed to zero, and far from them it is unchanged. Approximately, a region of size a around the crack is relieved of its elastic energy, and this energy release is insensitive to the particle size. However, when the particle size is reduced to be comparable to the crack size, the region of zero stress near the crack faces and accordingly that of elastic energy relief become dependent on the particle size. The smaller the particle is, the less the stress-relief volume, and the lower the elastic energy release. A crack will not extend if the driving force of strain energy release rate is less than the resistance of surface energy. This explains the observation of the critical particle size in averting fracture during lithiation experiments.

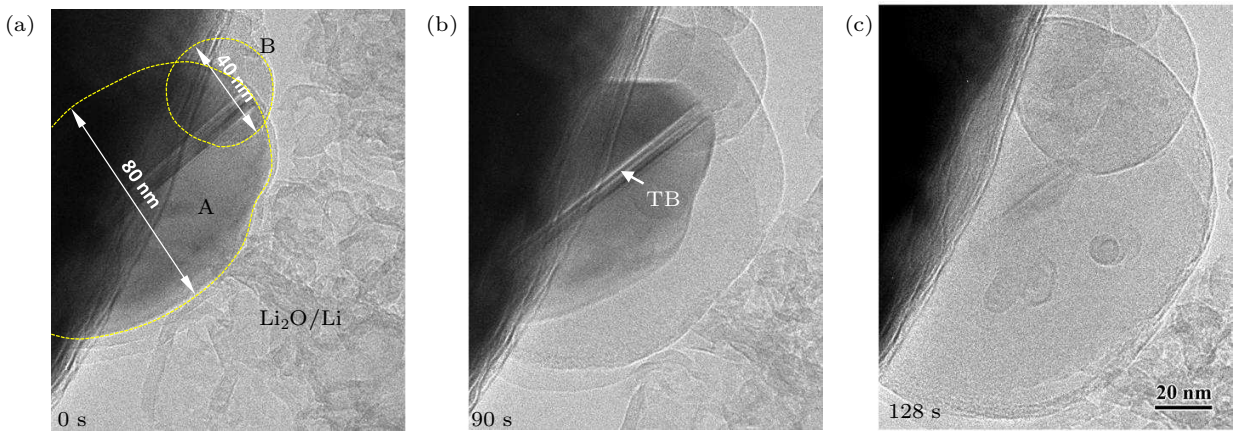

Fig. 7. *In situ* TEM observation of lithiation of two small c-Si nanoparticles without fracture.[17] (a) Two pristine c-Si nanoparticles, marked by "A" and "B" with diameters of 80 and 40 nm, respectively. There is a twin boundary (TB) in the center of particle A. (b) A partially lithiated state with a core–shell, two-phase microstructure in the two nanoparticles. (c) Neither cracking nor fracture occur in the two Si nanoparticles after full lithiation, and but both nanoparticles have $\sim 280\%$ volume expansion.

4. Mechanical properties

In order to understand and mitigate the mechanical degradation in LIBs, it is essential to quantitatively characterize the fundamental mechanical properties of high-capacity electrode materials. Using Si as an example, here we review recent progress in the quantitative experimental characterization of mechanical properties of Li–Si alloys, which involve a large range of Li:Si ratio from 0 to 3.75.

Hertzberg *et al.* conducted the nanoindentation testing on polycrystalline Si thin films at various stages of lithiation.[34] They reported a strong dependence of Young's modulus and hardness on the Li to Si ratio. Young's modulus was found to decrease from an initial value of 92 GPa for pure Si to 12 GPa for $Li_{3.75}Si$, and the hardness changes from 5 GPa to 1.5 GPa, correspondingly. Chon *et al.* used the curvature measurement technique to determine the yield stress in a lithiated Si thin film.[16] They reported a yield stress of 0.5 GPa for a-$Li_{3.5}Si$, and other thin film lithiation experiments reported similar values.[35] Kushima *et al.* measured the fracture strength and plasticity of lithiated Si nanowires by *in situ* TEM tensile testing.[36] The tensile strength decreased from the initial value of about 3.6 GPa for pristine Si nanowires to 0.72 GPa for a-Li_xSi ($x \sim 3.5$) nanowires. They also reported the large fracture strains that range from 8%–16% for a-Li_xSi ($x \sim 3.5$) nanowires, 70% of which remained unrecoverable after fracture. Pharr *et al.* measured the fracture energy of lithiated Si thin-film electrodes as a function of Li concentration. The fracture energy was determined to be $\Gamma = 8.5 \pm 4.3$ J/m^2 at small Li concentrations ($\sim Li_{0.7}Si$) and has bounds of $\Gamma = 5.4 \pm 2.2$ J/m^2 to $\Gamma = 6.9 \pm 1.9$ J/m^2 at larger Li concentrations ($\sim Li_{2.8}Si$). Recently, Wang *et al.* performed fracture toughness measurements by nanoindentation on lithiated a-Si thin films.[37] Their results showed a rapid brittle-to-ductile transition of fracture as the Li:Si ratio was increased to above 1.5. They reported the fracture energy of a-Si as 2.85 ± 0.15 J/m^2 and $Li_{1.09}Si$ as 8.54 ± 0.72 J/m^2, respectively.

It is important to note that several recent experimental studies have measured the time-dependent mechanical properties of lithiated Si. Boles *et al.* conducted uniaxial tensile and creep testing of fully lithiated Si nanowires.[38] Their creep testing was performed at fixed force levels above and below the tensile strength of the material. A linear dependence of the strain rate on the applied stress was evident below the yield stress of the alloy, indicating viscous deformation behavior. Pharr *et al.* also studied the rate effect on stress generation in Si thin films.[39] They varied the rate of lithiation of a-Si thin films and simultaneously measured stresses. An increase in the rate of lithiation resulted in a corresponding increase in the flow stress. These observations indicate that rate-sensitive plasticity occurs in a-Li_xSi electrodes at room temperature and at charging rates typically used in LIBs. Recently, Berla *et al.* studied the time-independent and time-dependent mechanical behavior of electrochemically lithiated

Si with nanoindentation.[40] Their nanoindentation creep experiments demonstrated that lithiated Si creeps readily, with the observed viscoplastic flow governed by power law creep with large stress exponents (> 20). This research emphasizes the importance of incorporating viscoplasticity into lithiation/delithiation models.

The mechanical properties of a-Li$_x$Si alloys have also been studied using quantum mechanical and interatomic potential calculations. Shenoy *et al.* performed the density functional theory (DFT) calculations of the elastic properties of a-Li$_x$Si alloys.[41] They showed the elastic softening with increasing Li concentration. Zhao *et al.* conducted DFT calculations for both the biaxial yield stress in a-Li$_x$Si thin films and the uniaxial yield stress in bulk a-Li$_x$Si under tension.[42] They found large differences between the characteristic yield stress levels of the two cases. Cui *et al.* developed a modified embedded atomic method (MEAM) interatomic potential for the Li$_x$Si alloys.[43] They performed molecular dynamics simulations of uniaxial tension for bulk a-Li$_x$Si at 300 K and showed that the yield strength decreased from about 2 GPa for a-LiSi to 0.5 GPa for a-Li$_{3.75}$Si. Fan *et al.* performed molecular dynamics simulations to characterize the mechanical properties of a-Li$_x$Si with a reactive force field (ReaxFF).[44] They computed the yield and fracture strengths of a-Li$_x$Si alloys under a variety of chemo-mechanical loading conditions. The effects of loading sequence and stress state were investigated to correlate the mechanical responses with the dominant atomic bonding, featuring a transition from the covalent glass to the metallic glass characteristics with increasing Li concentration. In addition, quantum mechanical calculations have been performed to study the atomic structures and energetics associated with Li diffusion and reaction in a-Li$_x$Si alloys.[45–53] The aforementioned modeling studies not only provide valuable insights into the mechanical properties of a-Li$_x$Si, but also highlight the challenges to understand the structure-property relationship in a-Li$_x$Si. Namely, the composition and structure can change drastically during electrochemical cycling of Si electrodes, involving for example the transition from a Li-poor network glass to a Li-rich metallic glass with increasing Li concentration during lithiation.[54,55]

5. Conclusions and future research directions

In conclusion, the mechanics of LIBs is an emerging and exciting research field. Mitigation of mechanical degradation in high-capacity electrode materials is one of the principal challenges facing the development of next-generation high performance LIBs. Among a vast list of potentially intriguing directions for future research, several areas present particularly pressing needs.

(i) It is critical to develop the new experimental techniques to characterize and quantitatively measure the mechanical responses of battery materials at different length and time scales. In this review, we have focused on recent advances in the *in situ* stress measurement by thin film electrodes and the *in situ* TEM experiment of nanomaterial electrodes. However, there are still a large number of dynamic, electro-chemo-mechanical processes and properties that need to be quantitatively characterized at different scales, but are not accessible by existing experimental tools.

(ii) The development of chemomechanical theories and models is highly desired, but they should be closely coupled with experiments whenever possible. The past few years have seen a dramatic increase in the new non-linear field theories and computational models for LIBs. However, the key challenges and opportunities reside in their capability of being predictive. To this end, the non-linear field theories and computational models should be closely related to the high-fidelity experiments in the future research. This is because gaining the predictive capability is hinged on a deep understanding of the controlling chemomechanical mechanisms that need to be directly revealed and clarified through high-fidelity experiments.

(iii) It is necessary to study the mechanical behavior of SEIs, which are widely recognized to play a key role in controlling the battery performance and cycle life. While SEIs have been studied for several decades, their exact microstructure and mechanical properties remain unclear. Recently, Zheng *et al.* used the scanning force spectroscopy to map the morphologies and mechanical responses of a thin SEI layer formed on the surface a Si thin film electrode.[56] Their results revealed the high non-uniformity of film thickness and Young's modulus in SEIs. While their work is a new step towards understanding the mechanics of SEIs, much effort needs to be dedicated to the study of mechanics of SEIs in the future.

(iv) It is imperative to apply the knowledge, data and insights gained from the fundamental mechanics research to the design of durable LIBs. In this regard, we note that various strategies such as coatings,[57] hollow geometries,[58] and hierarchical structures[59] are being used to mitigate the mechanical degradation and capacity fade in high-capacity electrodes. However, the mechanics of lithiation/delithiation in these systems remain poorly understood. For example, during lithiation of a hollow Si nanotube, it is possible to generate the outward displacement at the outer surface and the outward/inward displacement at the inner surface of the nanotube. Knowing the signs and relative magnitudes of those displacements are critical for designing the durable coatings and finding means to stabilize SEIs. The existing models with various assumptions have yielded different predictions.[58,60] A careful *in situ* study is critically needed to clarify the mechanics and mechanism in lithiated hollow Si nanotubes.

(v) Understanding the physics of lithiation and delithiation in high-capacity electrodes is essential to advance the

battery field. There are a number of puzzling observations during *in situ* TEM studies. For example, nanoscale *a*-Si underwent the two-phase and two-stage mechanism during the first lithiation.[18] However, there was no clearly visible phase boundary during the second lithiation. Moreover, *a*-Si cannot be further lithiated/delithiated during a typical *in situ* TEM experiment after about ten cycles. Resolving these puzzles requires a fundamental understanding of the thermodynamics, kinetics, atomic structures, and mechanisms of the reaction and diffusion processes in multiphase alloys under coupled electrochemical and mechanical loadings.[61,62]

Finally, we note that tackling the above mechanics problems presents many challenges and opportunities for experimentalists and modelers to work together. Hopefully, the synergistically integrated experiment and modeling will help understand, control, and optimize the mechanical behavior of electrodes, SEIs, and cell systems, thereby enabling the development of high-performance LIBs.

References

[1] Tarascon J M and Armand M 2001 *Nature* **414** 359
[2] Dunn B, Kamath H and Tarascon J M 2011 *Science* **334** 928
[3] Goodenough J B and Kim Y 2010 *Chem. Mater.* **22** 587
[4] Huggins R A and Nix W D 2000 *Ionics* **6** 57
[5] Beaulieu LY, Eberman K W, Turner R L, Krause L J and Dahn J R 2001 *Electrochem. Solid State Lett.* **4** A137
[6] Chan C K, Peng H L, Liu G, McIlwrath K, Zhang X F, Huggins R A and Cui Y 2008 *Nat. Nanotech.* **3** 31
[7] Cheng Y T and Verbrugge M W 2009 *J. Power Sources* **190** 453
[8] Zhao K, Pharr M, Vlassak J J and Suo Z 2010 *J. Appl. Phys.* **108** 073517
[9] Sethuraman V A, Chon M J, Shimshak M, Srinivasan V and Guduru P R 2010 *J. Power Sources* **195** 5062
[10] Liu X H, Wang J W, Huang S, Fan F, Huang X, Liu Y, Krylyuk S, Yoo J, Dayeh S A, Davydov A V, Mao S X, Picraux S T, Zhang S, Li J, Zhu T and Huang J Y 2012 *Nat. Nanotech.* **7** 749
[11] Cui Z, Gao F and Qu J 2012 *J. Mech. Phys. Solid.* **60** 1280
[12] Gao Y F and Zhou M 2011 *J. Appl. Phys.* **109** 014310
[13] Purkayastha R and McMeeking R M 2012 *J. Appl. Mech. - Trans. ASME* **79** 031021
[14] Li H, Huang X J, Chen L Q, Wu Z G and Liang Y 1999 *Electrochem. Solid State Lett.* **2** 547
[15] Liu X H, Zheng H, Zhong L, Huang S, Karki K, Zhang L Q, Liu Y, Kushima A, Liang W T, Wang J W, Cho J H, Epstein E, Dayeh S A, Picraux S T, Zhu T, Li J, Sullivan J P, Cumings J, Wang C, Mao S X, Ye Z Z, Zhang S and Huang J Y 2011 *Nano Lett.* **11** 3312
[16] Chon M J, Sethuraman V A, McCormick A, Srinivasan V and Guduru P R 2011 *Phys. Rev. Lett.* **107** 045503
[17] Liu X H, Zhong L, Huang S, Mao S X, Zhu T and Huang J Y 2012 *ACS Nano* **6** 1522
[18] Wang J W, He Y, Fan F, Liu X H, Xia S, Liu Y, Harris C T, Li H, Huang J Y, Mao S X and Zhu T 2013 *Nano Lett.* **13** 709
[19] McDowell M T, Lee S W, Harris J T, Korgel B A, Wang C, Nix W D and Cui Y 2013 *Nano Lett.* **13** 758
[20] McDowell M T, Lee S W, Nix W D and Cui Y 2013 *Adv. Mater.* **25** 4966
[21] Woodford W H, Chiang Y M and Carter W C 2010 *J. Electrochem. Soc.* **157** A1052
[22] Haftbaradaran H, Xiao X C, Verbrugge M W and Gao H J 2012 *J. Power Sources* **206** 357
[23] Wang H, Hou B, Wang X, Xia S and Chew H B 2015 *Nano Lett.* **15** 1716
[24] Trattnig G and Leitgeb W 2014 Battery Modelling for Crash Safety Simulation InAutomotive Battery Technology (ed. Thaler A and Watzenig D) p. 19
[25] Liu X H, Liu Y, Kushima A, Zhang S L, Zhu T, Li J and Huang J Y 2012 *Adv. Energy Mater.* **2** 722
[26] Liu Y, Zhang S and Zhu T 2014 *Chemelectrochem.* **1** 706
[27] Yan B, Lim C, Yin L and Zhu L 2012 *J. Electrochem. Soc.* **159** A1604
[28] Huang J Y, Zhong L, Wang C M, Sullivan J P, Xu W, Zhang L Q, Mao S X, Hudak N S, Liu X H, Subramanian A, Fan H Y, Qi L A, Kushima A and Li J 2010 *Science* **330** 1515
[29] Liu Y, Zheng H, Liu X H, Huang S, Zhu T, Wang J W, Kushima A, Hudak N S, Huang X, Zhang S L, Mao S X, Qian X F, Li J and Huang J Y 2011 *ACS Nano* **5** 7245
[30] Huang S, Fan F, Li J, Zhang S L and Zhu T 2013 *Acta Materialia* **61** 4354
[31] Liu X H, Fan F, Yang H, Zhang S, Huang J Y and Zhu T 2013 *ACS Nano* **7** 1495
[32] McDowell M T, Ryu I, Lee S W, Wang C, Nix W D and Cui Y 2012 *Adv. Mater.* **24** 6034
[33] Gu M, Yang H, Perea D E, Zhang J G, Zhang S and Wang C M 2014 *Nano Lett.* **14** 4622
[34] Hertzberg B, Benson J and Yushin G 2011 *Electrochem. Commun.* **13** 818
[35] Soni S K, Sheldon B W, Xiao X C, Verbrugge M W, Ahn D, Haftbaradaran H and Gao H J 2012 *J. Electrochem. Soc.* **159** A38
[36] Kushima A, Huang J Y and Li J 2012 *ACS Nano* **6** 9425
[37] Wang X, Fan F, Wang J, Wang H, Tao S, Yang A, Liu Y, Chew H B, Mao S X, Zhu T and Xia S 2015 *Nat. Commun.* **6** 8417
[38] Boles S T, Thompson C V, Kraft O and Moenig R 2013 *Appl. Phys. Lett.* **103** 263906
[39] Pharr M, Suo Z and Vlassak J J 2014 *J. Power Sources* **270** 569
[40] Berla L A, Lee S W, Cui Y and Nix W D 2015 *J. Power Sources* **273** 41
[41] Shenoy V B, Johari P and Qi Y 2010 *J. Power Sources* **195** 6825
[42] Zhao K J, Tritsaris G A, Pharr M, Wang W L, Okeke O, Suo Z G, Vlassak J J and Kaxiras E 2012 *Nano Lett.* **12** 4397
[43] Cui Z W, Gao F, Cui Z H and Qu J M 2012 *J. Power Sources* **207** 150
[44] Fan F, Huang S, Yang H, Raju M, Datta D, Shenoy V B, van Duin A C T, Zhang S and Zhu T 2013 *Modelling and Simulation in Materials Science and Engineering* **21** 074002
[45] Chevrier V L and Dahn J R 2009 *J. Electrochem. Soc.* **156** A454
[46] Chevrier V L and Dahn J R 2010 *J. Electrochem. Soc.* **157** A392
[47] Zhang Q F, Zhang W X, Wan W H, Cui Y and Wang E G 2010 *Nano Lett.* **10** 3243
[48] Huang S and Zhu T 2011 *J. Power Sources* **196** 3664
[49] Kim H, Chou C Y, Ekerdt J G and Hwang G S 2011 *J. Phys. Chem. C* **115** 2514
[50] Johari P, Qi Y and Shenoy V B 2011 *Nano Lett.* **11** 5494
[51] Zhao K J, Wang W L, Gregoire J, Pharr M, Suo Z G, Vlassak J J and Kaxiras E 2011 *Nano Lett.* **11** 2962
[52] Chan M K Y, Wolverton C and Greeley J P 2012 *J. Am. Chem. Soc.* **134** 14362
[53] Jung S C, Choi J W and Han Y K 2012 *Nano Lett.* **12** 5342
[54] Argon A S and Demkowicz M J 2008 *Metall. Mater. Trans. A* **39A** 1762
[55] Schuh C A, Hufnagel T C and Ramamurty U 2007 *Acta Mater.* **55** 4067
[56] Zheng J, Zheng H, Wang R, Ben L, Lu W, Chen L, Chen L and Li H 2014 *Phys. Chem. Chem. Phys.* **16** 13229
[57] Zhang LQ, Liu X H, Liu Y, Huang S, Zhu T, Gui L J, Mao S X, Ye Z Z, Wang C M, Sullivan J P and Huang J Y 2011 *ACS Nano* **5** 4800
[58] Wu H, Chan G, Choi J W, Ryu I, Yao Y, McDowell M T, Lee S W, Jackson A, Yang Y, Hu L B and Cui Y 2012 *Nat. Nanotech.* **7** 310
[59] Wu F, Lee J T, Fan F, Nitta N, Kim H, Zhu T and Yushin G 2015 *Adv. Mater.* **27** 5579
[60] Jia Z and Li T 2015 *J. Power Sources* **275** 866
[61] Gosele U and Tu K N 1982 *J. Appl. Phys.* **53** 3252
[62] Gosele U and Tu K N 1989 *J. Appl. Phys.* **66** 2619